Quantitative Assessment of Secondary Flows of Single-phase Fluid through Pipe Bends

Z. Kaldy[1], O. Ayala[1]*
[1] Engineering Technology Department, Old Dominion University, Norfolk VA, USA
*oayala@odu.edu

Abstract: Single-phase fluid flow was simulated passing through various three dimensional pipe elbows. The simulations varied by Reynolds number, curvature ratios, and sweep angles and were all conducted using the k-ε model available in COMSOL Multiphysics 5.1. The intent of this research was to qualitatively assess the flow characteristics under several different conditions. Many similarities were seen especially when comparing curvature ratios, the vorticity location for the turbulent cases show near identical behavior at the elbow midsection. One of the variables quantified in this paper is the maximum secondary velocity module which shows increasing values until the midsection of the elbow.

Keywords: Single-phase flow, Secondary flow, Vorticity, Pipe bend, Pipe elbow

1. Introduction

There are hundreds of processes within the industry where a fluid is required to pass through a pipeline system. Due to particle contamination within these fluids, erosion in the piping system is a concern. Replacement of eroded pipes is one of the major costs of maintenance, which is an obvious pitfall in the overall cost of operation in industries. The highest erosion rate is most commonly found in bends, as fluid particles are dragged towards the wall due to the streamwise and secondary flows. A better understanding of the secondary flows is required to gauge their impact in the particle trajectories.

Most of the studies concerning secondary flows have focused on a more qualitative assessment through visualization of their streamlines, velocity contours, and velocity vectors (e.g., Sudo et al., 1997; Timité et al, 2009; Röhrig et al. 2015). In this research, we will focus on a more quantitative assessment of the secondary flows by measuring the flow intensity, vorticity magnitude (maximum, and their locations), maximum secondary velocity module, and mean secondary flow velocity. Some of these parameters have been previously used in studies with settings different to the ones considered here. Kim et al. (2014) and Wang et al. (2015) looked into the swirl intensity and secondary flow intensity for small curvature radius bend and a straight pipe after a 90˚elbow respectively. Boiron et al. (2007) looked at the maximum secondary flow velocity when analyzing an oscillatory flow in a U-bend. Vorticity magnitudes and location of core vortex were observed by Sudo et al. (1992), Vester et al. (2015), and Hellström et al. (2013) to study oscillatory flow in a curved pipe and a flow downstream of a 90˚bend.

We propose to analyze how all those parameters of the secondary flows evolve along the bends for: four different Reynolds numbers (100; 1,000; 10,000; and 100,000), three curvature ratios (r/D: 1.5, 6.5, and 10), and three sweep angles (22.5, 45, and 90 degrees). The computational fluid dynamics software used was COMSOL Multiphysics 5.1 through its CFD module.

2. Physical Model

All of the simulations included in this study used a pipe diameter of 1 inch (0.0254 [m]) with variations on other parameters such as sweep angle (θ), curvature ratio (γ), and Reynolds number (Re). An entrance length (Le) of 2.3 [ft] (0.7 [m]) was used to allow the flow to develop before entering the pipe elbow. The length of 2.3 [ft] (0.7 [m]) was also used for the exit length (Lo) to ensure no flaws due to outlet conditions.

To decrease computational time and efforts the model was simplified in a number of ways. Due to there being only one working fluid there is no difference in density between one particle and another hence the elimination of gravitational forces. Since gravitational forces were neglected there are also no buoyancy forces.

The mesh was created based off of the most involved simulation that was computed (Re = 100,000; $\gamma = 1.5$; $\theta = 90^{\circ}$); the idea being that the mesh would be adequate and fine enough to calculate, with minimal error, all of the cases

studied. A tetrahedral mesh was used, however the boundary layers near the wall are thin rectangular elements; this is so that the computational resources are spared and so that the velocity gradients near the wall can be computed more accurately for the turbulent cases. The boundary layers were analyzed so that to choose an appropriate thickness, this thickness was determined to be 1.5E-4 [m] thick. Finally the mesh used for the domain of the pipe was created using the predefined mesh sizes within COMSOL. The various mesh options (Course, Normal, and Fine) were analyzed for data sensitivity.

3. Numerical Model & Flow

The studies encompassed in this research included both laminar and turbulent flow models which were provided using COMSOL Multiphysics. These models treat the fluid as it is a single-phase, incompressible, homogenous, Newtonian, and isothermal liquid, with the working fluid properties of water. The properties of the water used are density (ρ) and dynamic viscosity (μ), 999.84 [kg/m3] and 1.002E-3 [N/s-m^2] respectfully. Using the Bulk Reynolds number (Re), pipe diameter (D), density, and viscosity the average flow velocity ($\overline{U}$) was obtained. For the case of Re of 100,000 the equation results in a mean velocity of 3.95 [m/s] also shown in Table 1.

As the fluid velocity increases the flow becomes more turbulent and more difficult and time consuming to simulate. Two of the cases evaluated in this paper have velocities and therefore Reynolds numbers within the laminar domain (Re < 2100) and the other two cases have Reynolds numbers within the turbulent domain (Re > 4000).

4. Boundary Conditions & Model Validation

The equations solved, for both flow models, include the three dimensional Navier-Stokes equations for conservation of momentum and the continuity equation for conservation of mass. Due to the rate at which laminar flow develops it was unnecessary to obtain velocity profiles from preliminary simulations. Therefore, the flow had enough length of pipe to fully develop before entering the pipe elbow. However for the turbulent flow axial velocity profile the decision was made to run preliminary simulations to obtain data for a velocity profile. Ergo, the turbulent cases, including Re of 10,000 and 100,000, velocity profiles were derived from a preparatory simulation. After obtaining the data for the velocity profile the data was inputted and interpolated for the final simulations. This reduced the length of pipe required before the elbow thus reducing the computational time required for each simulation.

Since the main interest in these simulations is the intensity and location of the dean vortices and since Hellström et al. (2013) noted phenomena such as swirl switching effect, the entire domain of the pipe and pipe elbow had to be simulated. If only half of the geometry is simulated this phenomenon would not be apparent, not allowing for more realistic results.

At the outlet of the pipe the pressure controlled boundary condition is used. The pressure over the entire outlet section of the pipe is set to 0 [pa]. Since this condition was enforced some numerical errors might be produced which are concentrated near the outlet of the pipe. Therefore no data was collected or analyzed after four pipe diameters downstream of the pipe elbow.

Since we have two models to simulate (Laminar and Turbulent) there are different settings for the wall boundary conditions. As for the laminar case the “No Slip” function was used. Meaning that the fluid along the edge of the wall will be represented by a magnitude of zero since the wall is stationary. As for the turbulent simulations the “Wall Functions” boundary condition was used which gives a magnitude of axial velocity at the wall that represents the magnitude of the velocity at the most inner boundary layer.

The results of Homicz (2004) were replicated using COMSOL Multiphysics as to validate and verify that the current method produces similar results. The geometry was duplicated and all boundary conditions were matched. Finally the simulation was conducted and the results were analyzed in the same manner as was done by Homicz (2004). Although there were some minor discrepancies between the two simulations they were within reasonable agreement with one another.

5. Results and Discussion

To better visualize the results of the simulations the data was normalized to transform the results into non-dimensional values. Both the velocity and the vorticity plots have been normalized with Umean* and Umean*/D, respectfully. For both the laminar and turbulent cases Umean* is simply half of the average velocity solved for using the bulk Reynolds number equation also shown in Table 1.

Table 1. Normalization Factors (Umean*)

Re	Umean [m/s]	Umean* [m/s]	Arrow scales
100	0.00354	0.00177	1
1,000	0.0354	0.0177	0.15
10,000	0.354	0.177	0.025
100,000	3.54	1.77	0.0025

It is important to mention that the following plots have some similarities with respect to the way they were analyzed. All simulations with identical Reynolds numbers have arrows plotted which are all scaled equally, however from one Reynolds number to the next they are not identical.

Variations were made to the geometry to make comparisons between different models and various Reynolds numbers. In this section the results were reviewed using tabulated results and cross sectional plots of the geometry taken at selected intervals. The plots shown are rotated in such a manner that the inside of the bend is towards the left side of the circle (+ θ) and the outside of the bend is towards the right (- θ) as shown in Figure 4.

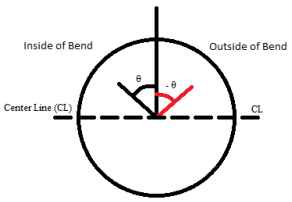

Figure 2 Layout of Plots and Data

When the flow passes through the elbow multiple characteristics play a part in how and why the fluid moves as it does. One of the motions observed is the axial flow which is simply described as the bulk flow of the fluid passing from inlet to outlet. The other flow observed is what is called the "secondary flow" which forms as two counter-rotating vortical structures. These structures are best seen in Table 2 row (I) which shows the axial flow and secondary flow streamlines. The vorticity and in-plane velocity vector arrows, in row (II), show how the fluid is rotating about its own axis. As seen in the figures on row (I) the axial flow is represented by a colored surface with warmer colors corresponding to higher velocities. The vorticity in row (II) is plotted as a surface with the warm colors (red-orange-yellow-green) spinning counter clockwise and the cool colors (dark blue-light blue-green) spinning clockwise. The in-plane velocity or secondary flow is represented by an arrow surface with proportional lengths set to the arrows to better understand where the flow is strongest. Section (A) of Table 2 is a comparison of the four different Reynolds numbers, section (B) is a comparison of the different sweep angles evaluated, and section (C) is a comparison of the three different curvature ratios assessed. Next is Table 3 which simply tabulates the various parameters of interest for the eight cases shown in Table 2.

5.1. General Analysis

One trait that all of the simulations seem to have in common is the off centered axial velocity at the beginning, middle, end, and even downstream the elbow exit. The reason for this shifted peak is due to the fluid being a continuous flow, meaning, when fluid particles downstream or upstream of a flow are altered the neighboring fluid particles feel a slightly smaller force. This is mainly due to the fluid being an incompressible, if the fluid had been air the fluid particles would act more independently.

Although the fluid used was a continuous fluid the impact of the continuity did not cascade all the way back to the beginning of the elbow with respect to the secondary flow. The reason the vorticity plots were omitted for the cross section at the beginning of the pipe elbow is because there were no visible or measurable differences between the various elbow inlets. Also omitted from the plots are the cross sectional cuts 1D, 2D, and 4D downstream of the elbow. Those plots were omitted because of the similarities between one another. The secondary flow and vorticity is better compared at and after half way through the pipe elbow. When the fluid

Table 2 A comprehensive table for comparison. The top two rows represent axial flow and the bottom two rows represent vorticity. (A) Comparison between Reynolds numbers. (B) Comparison between Sweep Angles (C) Comparison between Curvature Ratios

		Reynolds Number (Re) [$\gamma = 1.5$, $\theta = 90^\circ$]				Sweep Angle (θ) [Re = 10,000; $\gamma = 1.5$]			Curvature Ratio (γ) [Re = 100,000; $\theta = 90$]			
		100,000	10,000	1,000	100	90	45	22.5	1.5	6.5	10	
(I)	Elbow Midsection	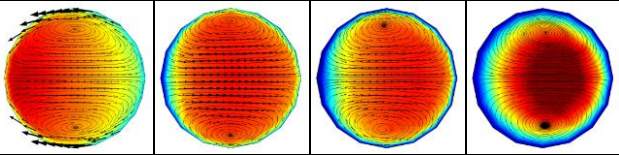				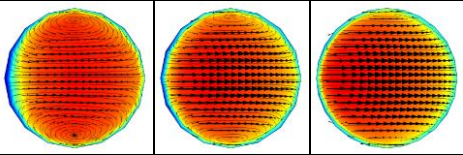			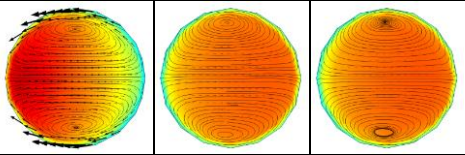			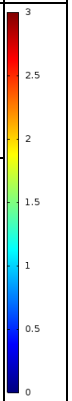
	Elbow End	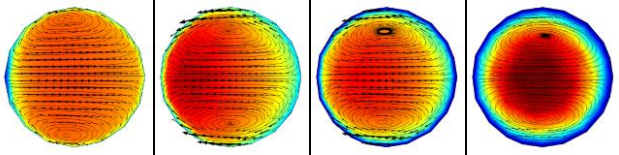				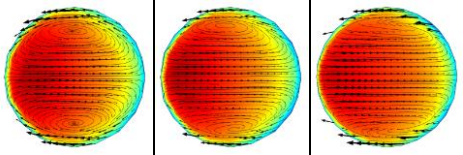			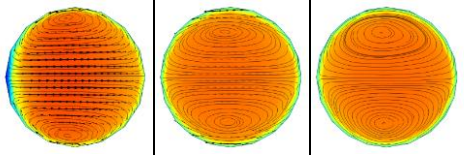			
(II)	Elbow Midsection	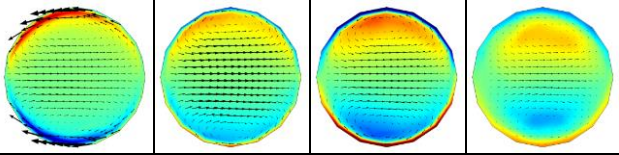				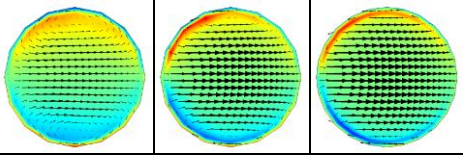			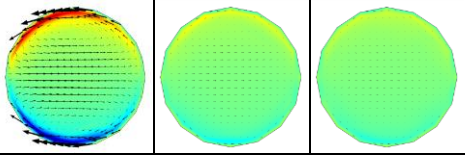			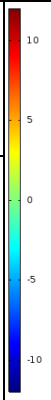
	Elbow End	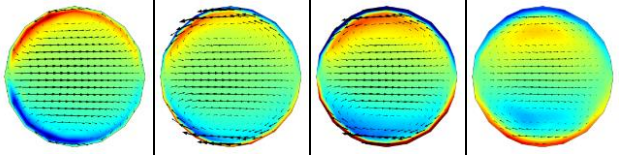				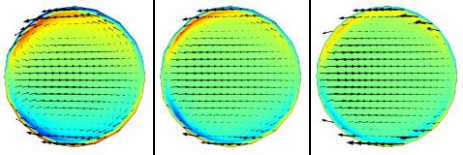			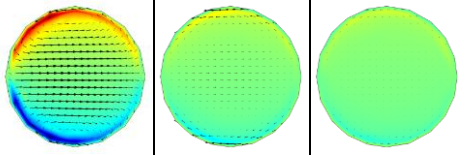			
		(A)				(B)			(C)			

Table 3 Data for simulations presented on Table 2
(Highlighted are the maximum values within each simulation)

			Mean Axial Velocity $\left[\overline{U}\right]$ [m/s]	Max In-Plane Velocity [m/s]	$\frac{U\ \max}{\overline{U}}$	Maximum Vorticity [1/s]	Location	
							r [m]	θ [deg]
1	Re = 100K γ = 1.5 θ = 90	0 [deg]	3.95	0.50174	0.1270			
		45 [deg]		1.9899	0.5038	888.10	0.0119	17.5
		90 [deg]		1.08009	0.2734	1024.70	0.0119	22.4
		1D		0.60178	0.1523	256.05	0.0116	52.8
		2D		0.383144	0.0970	142.78	0.0108	32.3
		4D		0.1872	0.0474	73.65	0.0105	45.0
2	Re = 100K γ = 6.5 θ = 90	0 [deg]	3.95	0.17915	0.0454			
		45 [deg]		0.72639	0.1839	288.02	0.0118	20.5
		90 [deg]		0.315492	0.0799	335.33	0.0119	22.5
		1D		0.19199	0.0486	65.72	0.0112	11.6
		2D		0.13132	0.0332	43.60	0.0102	17.3
		4D		0.073613	0.0186	25.62	0.0101	19.2
3	Re = 100K γ = 10 θ = 90	0 [deg]	3.95	0.15231	0.0386			
		45 [deg]		0.25438	0.0644	187.07	0.0119	0.0
		90 [deg]		0.25936	0.0657	173.54	0.0119	22.5
		1D		0.16642	0.0421	61.06	0.0112	5.5
		2D		0.10782	0.0273	42.30	0.0103	-16.9
		4D		0.081286	0.0206	23.06	0.0103	7.5
4	Re = 10K γ = 1.5 θ = 90	0 [deg]	0.395	0.051572	0.1306			
		45 [deg]		0.15443	0.3910	63.20	0.0116	31.2
		90 [deg]		0.11655	0.2951	46.23	0.0116	22.4
		1D		0.049049	0.1242	17.51	0.0098	37.1
		2D		0.027904	0.0706	8.72	0.0096	-0.9
		4D		0.011415	0.0289	3.32	0.0100	21.4
5	Re = 10K γ = 1.5 θ = 45	0 [deg]	0.395	0.048251	0.1222			
		22.5 [deg]		0.1368	0.3463	61.52	0.0119	34.1
		45 [deg]		0.19145	0.4847	76.25	0.0119	45.0
		1D		0.067048	0.1697	14.15	0.0099	22.8
		2D		0.032423	0.0821	6.02	0.0100	36.8
		4D		0.018193	0.0461	1.66	0.0108	27.5
6	Re = 10K γ = 1.5 θ = 22.5	0 [deg]	0.395	0.041351	0.1047			
		11.25 [deg]		0.16905	0.4280	32.63	0.0119	47.0
		22.5 [deg]		0.20866	0.5283	92.46	0.0119	46.3
		1D		0.070407	0.1782	12.24	0.0107	26.8
		2D		0.040671	0.1030	4.84	0.0104	12.5
		4D		0.012036	0.0305	1.75	0.0100	-7.4
7	Re = 1K γ = 1.5 θ = 90	0 [deg]	0.0395	0.005117	0.1295			
		45 [deg]		0.022922	0.5803	5.85	0.0107	26.1
		90 [deg]		0.013305	0.3368	5.68	0.0107	12.8
		1D		0.0067318	0.1704	1.94	0.0096	37.4
		2D		0.0033499	0.0848	1.04	0.0078	2.8
		4D		0.0014049	0.0356	0.33	0.0087	3.1
8	Re = 100 γ = 1.5 θ = 90	0 [deg]	0.00395	0.00051575	0.1306			
		45 [deg]		0.0017538	0.4440	0.32	0.0081	8.4
		90 [deg]		0.001403	0.3552	0.34	0.0080	25.7
		1D		0.00037975	0.0961	0.10	0.0071	-14.0
		2D		0.00013363	0.0338			
		4D		0.00011435	0.0289			

first enters the elbow it has already begun to react to the sweep angle of the elbow as the core of the axial velocity moves toward the inside of the bend. Once the fluid begins to make the turn, centrifugal forces and secondary flows are initiated causing an imposed vortical structure to form on either side of the centerline. These vortical structures start forming close to the walls as the flow enters the elbow and move closer to the center of the pipe as the flow continues through the elbow. This phenomenon will be described in a later section of this paper.

5.2. Effect of Reynolds Number

The preceding two tables (Table 2 Column A and Table 3 Rows: 1, 4, 7, and 8) show a comparison of four simulations with identical geometry and a variation of Reynolds numbers. The model selected has a sweep angle of 90 °, a curvature ratio of 1.5 and the four Reynolds numbers simulated (100K, 10K, 1K, 100).

As shown on these plots the secondary flow formed within the pipe, as the fluid passes through the elbow, generates two counter-rotating vortices. However as the Reynolds number decreases the location of the core of the two vortical structures changes. When comparing the 100K simulation to the 100 it is apparent that the structures move away from the walls of the pipe at lower Reynolds numbers. As shown in Table 3 the magnitude of the vorticity decreases as the Reynolds number decreases.

The reason the vorticity stays closer to the wall for higher Reynolds numbers is due to the inertial forces of the fluid. Since the Reynolds number is the ratio of the inertial forces over the viscous forces the higher the Reynolds' number the higher the inertial forces therefore the more resistant the structures are to change.

A common similarity between the differing Reynolds number simulations conducted is the behavior of the maximum secondary velocity module $\left(U_{max}/\overline{U}\right)$. As seen in row 1, 4, 7, and 8 of Table 3 the intensity of the secondary flow increases until reaching its maximum at the midsection of the elbow; though the location and magnitude of the vorticity differ.

5.3. Effect of Curvature Ratio

The initial thought behind changing the curvature ratio (γ) was that the larger the curvature ratio the longer the fluid had to develop within the elbow. Therefore as the fluid passed through the elbow it had more time to feel the effects of the centrifugal forces being imposed upon the flow. Although this is a good hypothesis it can be disproven by looking at rows 1, 2, and 3 of Table 3. As shown the fluid is exposed to both the highest vorticity and in-plane velocity magnitude during the pass through the pipe with a curvature ratio of 1.5. Despite the fact that vortical structures are still formed during the 6.5 and 10 they are not quite as strong as the structures formed during the 1.5. The reason behind this misleading hypothesis is due to the centrifugal acceleration felt by the fluid particles. Albeit the fluid experiences a longer time to develop with a larger curvature ratio it also experiences lower centrifugal acceleration which results in lower values of secondary flow velocity as well as vorticity.

5.4. Effect of Sweep Angles

Although changing the sweep angles gives more data to analyze making this study more complete there are only so many points to be made about this alteration. When comparing the elbow end plot of the 45 degree elbow with the midsection plot of the 90 degree elbow one would assume these plots to be identical. However since the fluid is continuous this is not the case. Due to the continuity of the fluid the fluid particles at the midsection of the 90 degree elbow are impacted by the fluid particles downstream at the elbow exit. Therefore the intensity of the secondary flow is continuing to develop as the fluid passes through the elbow. Although continuity is the main reason for these differences there are also computational mistakes that are to blame for the larger intensity at the midsection of the 22.5 degree elbow. When a vector is decomposed in this section it is impossible to differentiate the axial velocity with the in-plane velocity therefore skewing some results.

7. Conclusions

The most notable characteristics of the flow through a pipe elbow include the development and peak of the maximum secondary flow velocity module as well as the location and magnitude of the vorticity when comparing curvature ratios and Reynolds numbers respectfully. The most interesting part of the results for the comparison of curvature ratios is that the location of the vorticity at the elbow exit is nearly identical between the three simulations shown on Table 3 rows 1, 2, and 3 which show the location of $r = 0.0119$ and $\theta \approx 22.5$.

Another notable conclusion that can be drawn from the data on Table 3 is that the concentration of vorticity seems to be focused near the inside of the bend. This could be helpful when optimizing an elbow design that could reduce wall lift off. It is noted that the secondary flow and vorticity is strongly related to the Reynolds number and the curvature ratio.

One further simulation, not shown here, was conducted to interpret exactly where the secondary motion of fluid was occurring first. When analyzing the pressure contours across the midsection of the elbow, a higher pressure was seen towards the outside of the elbow which would cause the fluid to move from the outside of the elbow towards the inside. Since the fluid pathway towards the inside of the elbow is along the wall rather than the centerline there must be another force causing this motion. It is believed that the fluid is taking the path of least resistance which just happens to be within the boundary layer caused by the wall. Then once at the inside of the elbow the centrifugal forces are causing the fluid to fling towards the outside of the elbow and repeat this motion until the centrifugal forces and pressure gradients are no longer large enough to affect the fluid particles. Although this was a very inclusive and comprehensive study there is still future work to be done.

8. References

1. K. Sudo, et, al., Secondary motion of fully developed oscillatory flow in a curved pipe. *J. Fluid Mech.*, **237**, 189-208 (1992).
2. K. Sudo, et. al., Experimental investigation on turbulent flow in a circular-sectioned 90-degree bend. *Experiments in Fluids*, **25**, 42-49 (1998).
3. G. Homicz, Computational Fluid Dynamics Simulations of Pipe Elbow Flow. *Sandia National Laboratories Report*, **SAND2004-3467** (2004).
4. O. Boiron, et. al., Experimental and numerical studies on the starting effect on the secondary flow in a bend, *J. Fluid Mech.*, **274**, 109-129 (2007).
5. B. Timité, et. al., Pulsating Flow for Mixing in a Twisted Curved Pipe. *Journals of Fluids Engineering*, **131**, 121104-1-121004-10 (2009).
6. L. H. O. Hellström, et. al., Turbulent pipe flow downstream of a 90o bend. *J. Fluid Mech.*, **735**, R7-1-R7-11 (2013).
7. J. Kim, et. al., Characteristics of Secondary Flow Induced by 90-degree Elbow in Turbulent Pipe Flow, *Engineering Applications of Computational Fluid Mechanics*, **8**, 229-239 (2014).
8. A. K. Vester, et. al., POD analysis of the turbulent flow downstream a mild and sharp bend, *Exp Fluids*, **57**, 1-15 (2015).
9. R. Röhrig, et. al., Comparative computational study of turbulent flow in a 90o pipe elbow. *International Journal of Heat and Fluid Flow*, **55**, 120-131 (2015).
10. Y. Wang, et. al., Numerical Investigation on Fluid Flow in a 90-Degree Curved Pipe with Large Curvature Ratio, *Hindawi - Mathematical Problems in Engineering*, 1-12 (2015).

9. Acknowledgements

The authors would like to thank the Honors College/Office of Research for the academic and personal opportunity to work under the Program for Undergraduate Research and Scholarship (PURS) Grant at Old Dominion University.